Frequency Regulation of Multi-Area Power Systems with Plug-In Electric Vehicles Considering Communication Delays

Hua Fan[1], L. Jiang[2], Chuan-Ke Zhang[3,2,*], Chengxiong Mao[1]

[1]State Key Laboratory of Advanced Electromagnetic Engineering and Technology, Huazhong University of Science and Technology, Wuhan 430074, China.

[2]Department of Electrical Engineering & Electronics, University of Liverpool, Liverpool, L69 3GJ, United Kingdom

[3]School of Automation, China University of Geosciences, Wuhan 430074, China
[*]chuan-ke.zhang@liv.ac.uk

Abstract: Dynamics of vehicle-to-grid service to frequency regulation may suffer from the uncertainties arising from the spatial and temporal diversities of large number of plug-in vehicles (PEVs). Moreover, communication delays incurred in the aggregation of the PEVs, together with the ones in load frequency control (LFC) loop, will also degrade the dynamics and even destabilize the closed-loop system. This paper investigates the design of LFC scheme considering those uncertainties. Firstly, this paper develops a dynamic model of individual PEV based on Thevenin equivalent circuit and an aggregated model of group of PEVs considering uncertain driving behaviors, battery characteristics, and communication delays. Then, a state-space model with time delays and uncertainties is constructed to model the closed-loop LFC scheme with PEVs in primary control loop. After constructing the relationships among control gains, robust performances, and time delays, a robust PID-type LFC scheme design method is developed by using linear matrix inequality technique and particle swarm optimization algorithm. Case studies based on a three-area LFC system demonstrate that the PEVs can contribute to the frequency regulation under the step change and the long-term random load demands, and that the proposed LFC scheme achieves the suppressing of frequency fluctuations successfully in the presence of communication delays within the preset bounds and provides robustness against to the uncertainties arising from the PEVs and different load disturbances.

1. Introduction

In power system design and operation, the load frequency control (LFC) has been an important issue [1]. In traditional environment, the elimination of the frequency deviation and the power exchanges is achieved by adjusting the power output of generator units to track the demand changes. However with the development of smart grid, the increasing amount of renewable energies makes the problem more complicated. As a promising alternative to the internal combustion engine vehicles to reduce the greenhouse gas emission, plug-in electric vehicles (PEVs) have the potential to provide frequency support via the emerging vehicle-to-grid (V2G) technology, which has received many research efforts in recent years [2, 3, 4]. Numerous literature investigates the applications

of PEVs to providing frequency regulation services, mainly including the introduction of additional PEV-based primary frequency control (PFC) and PEV-based supplementary load frequency control.

In consideration of the quick response to frequency deviation, PEVs are easily used to construct an additional PFC loop, in which the charging/discharging power of PEVs is controlled by different V2G schemes with frequency deviation as the input signals. Large number of PEVs are aggregated to provide PFC by averaging the participation factor of PEVs in [5, 6]. In [7], PEVs are controlled to provide frequency regulation in a distributed manner and meanwhile satisfy the charging schedule set by vehicle users. In [8], a droop with dead band is applied to regulate the PEV charging/discharging power according to frequency signals. In [9], PEVs are applied to PFC based on distributed signal acquisition via limited communication. The decentralized V2G control method is proposed for PEVs to participate in PFC considering charging demands from PEV customers in [10]. The above mentioned literature sufficiently considers the uncertainty of V2G scheme, usually indicated by a time-varying V2G gain, caused by the spatiotemporal distribution of PEVs and the status of PEV, such as the travaling/parking time, the start charging time, the residual state of charge (SOC) of PEV's battery after each trip, the expected SOC, and the departure time of next trip, etc. The determination of the V2G gain requires the above realtime information, and the V2G output (deviation of charging/discharging power) depends upon the frequency deviations. Those signals are transmitted between aggregator and large number of PEV individuals, which may incur time delays (processing delay of calculation of V2G gain and transmission delay of frequency deviation) into the control loop. The field demonstration report shows that the delay between the aggregator and a PEV is less than several seconds when the wireless communication is used [11]. Among the previous mentioned works, the impact of the delays is only simply studied in [9] and thus requires deeper consideration. Moreover, how to redesign the LFC controller when the PEVs are included for frequency support is not considered in those literature.

Due to the utilization of aggregators for large-scale PEVs, PEVs can also participate in the supplementary frequency control responding to the ACE signals, instead of simple frequency deviation. In [12], a PID controller is designed for heat pump and PEVs to alleviate frequency fluctuation caused by intermittent power generation from wind farms. In [13], an LFC model including aggregated PEV battery storage has been proposed to improve the capability to incorporate wind power into the future Danish power system. In [14], a coordinated control scheme for large-scale PEVs and energy storage participating in the LFC service is studied. In [15], a robust LFC with coordinated V2G control is investigated. The work in [16] brings PEVs into the centralized LFC for interconnected power systems considering the PEVs charging demand. In [17], LFC of power systems with PEVs and diverse transmission links using distributed functional observers is discussed. As pointed in [19, 20, 21], closed-loop LFC system is a typical time-delay system due to the transmission of remote measurements to the control center and of control signals from the control center to the plant. However, most related researches considering the PEV-based supplementary LFC [12, 14, 15, 16] do not take into account the time delays, whose effect is only simply studied in [13]. Moreover, during the phase of designing LFC controllers in the above literature, the V2G scheme is usually considered as a very simple first-order transform function from the ACE signal to charging/dischanging power deviation with a constant V2G gain [12, 14, 17]. Such simplification cannot consider the uncertainties appearing in the V2G gain due to difference of the spatial/temporal distribution of the PEVs and the status of the PEV's battery.

Based on the aforementioned discussion, several issues, such as uncertainties of the V2G gain and the delays in LFC/PFC control loops, should be considered for the investigation of frequency

regulation of multi-area power systems with PEVs. This paper aims to design a robust PID-based LFC scheme for a multi-area power system by taking into account both the V2G gain uncertainty and the time delays. Note that the PEVs providing PFC service is considered in this paper due to their quick response to frequency deviation. Two aspects of improvements compared with the literature are made to achieve the objectives. On one hand, compared with the works of [8, 9, 10, 11] which only investigate the V2G gain of PEVs, this paper studies not only what the V2G gain is but also how to redesign the LFC scheme considering the PEVs. On the other hand, compared with the research of [12, 14, 17], in which very simple V2G gain is assumed to design the LFC scheme, this paper considers the uncertainties and the delays arising in the V2G scheme. More specifically, firstly, a linear state-space model with time delays and disturbances is constructed to model the closed-loop LFC scheme of each control area of the concerned power system. In the proposed model, the time delays in the control loops are modeled by some delayed state vectors; and the time-varying V2G gain of the PEVs are divided into two parts, one is a constant equal to the value with highest frequency of occurrence within the concerned time interval, and the other is the deviation between the constant value and the realtime V2G gain and regarded as a portion of the disturbances. Secondly, a distributed PID-based LFC scheme is designed for multi-area power systems with robustness against the V2G gain uncertainties and the time delays. In this scheme, the PID controller is tuned by combining a delay- and robust-performance-dependent PID controller tuning criterion, developed via the Lyapunov theory and the linear matrix inequality technique, and a standard particle swarm optimisation (PSO) algorithm.

The remainder of the paper is organized as follows. Section 2 gives the dynamic model of the concerned power system. Section 3 presents a robust PID controller tuning method for time-delay LFC systems. In Section 4, the effectiveness of the proposed method is verified by simulation studies on a typical three-area power system. Conclusions are given in Section 5.

2. Model of Power System with PEVs for Frequency Regulation

In this section, we discuss a dynamic model for frequency regulation of power systems with the PEVs and the distributed PID-type LFC scheme. The simplified model of individual PEV is developed based on the Thevenin equivalent circuit and the adaptive droop control [10]. The PEVs for supporting frequency regulation is finally modelled as a first-order transfer function, in which the heterogeneity of SOC of each PEV and the spatiotemporal diversities of all PEVs are indicated by a fixed aggregated V2G gain plus the bounded uncertainties. Finally, by considering the communication delays arising in the LFC loop and the aggregated PEVs loop, the state-space model of the power system with the PEVs is obtained by combing the proposed PEVs model and the dynamic model of traditional LFC scheme in [22].

2.1. Individual Grid-Connected PEV Model

The PEV provides V2G service through the charging/discharging of the battery, thus it requires to model the PEV battery to investigate PEV's contribution to frequency regulation. The PEV battery is connected to the distribution grid through the DC/AC inverter [9, 13], and its Thevenin equivalent circuit is shown in Fig. 1(a). The series resistor (R_s) describes the resistance of the battery terminal and inter-cell connections. The parallel RC network (R_t, C_t) describes the transient overvoltage effects. The open-circuit voltage $V_{\rm oc}(\rm SOC)$ is function of the SOC [13]. $V_{\rm cc}$ and $I_{\rm batt}$ are the battery DC current and voltage, respectively. The PEV charger is connected to the power grid

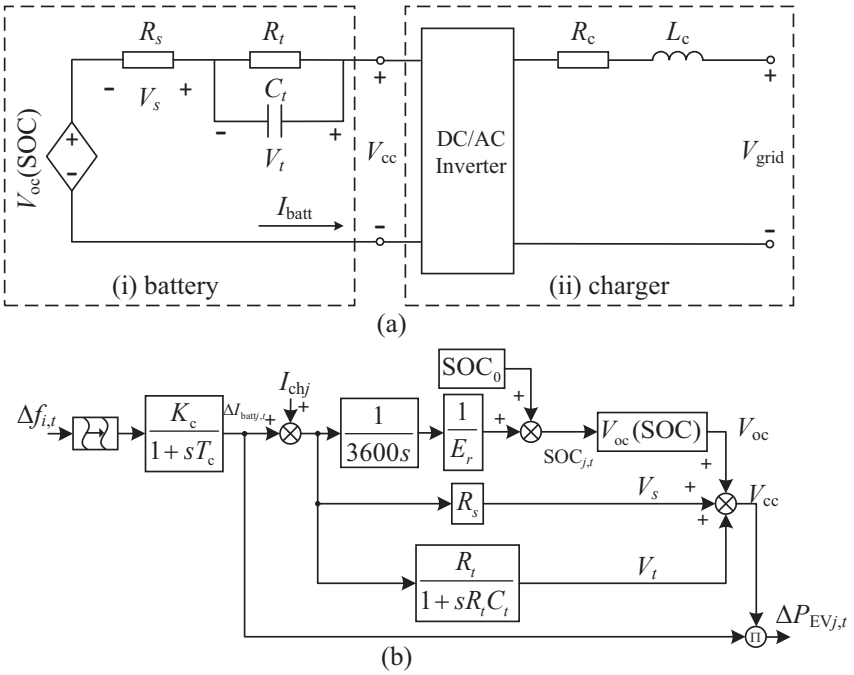

Fig. 1. *(a) Equivalent circuit of grid-connected PEV; (b) dynamic model of j-th PEV in PEVs Pool i*

through the resistor R_c and inductor L_c.

The PEV battery should be charged to satisfy the customers' drive requirements and provide the additional frequency regulation. The block diagram of dynamic model of the PEV is presented in Fig. 1(b).

Assume that the PEV is charged with constant current $I_{\mathrm{ch}j}$ in the unit of A, which can be obtained by [10]:

$$I_{\mathrm{ch}j} = \frac{\mathrm{SOC}_j^{\mathrm{d}} - \mathrm{SOC}_j^{\mathrm{in}}}{t_j^{\mathrm{out}} - t_j^{\mathrm{in}}} \cdot E_r \tag{1}$$

where $\mathrm{SOC}_j^{\mathrm{in}}$ and $\mathrm{SOC}_j^{\mathrm{d}}$ are the initial and desired SOC of the j-th PEV, respectively; t_j^{in} and t_j^{out} are the plug-in time and the plug-out time of the j-th PEV in the unit of hour; and E_r is the battery rated capacity in the unit of A-hour.

In Fig. 1(b), the first-order transfer function shows how the battery charging current changes with respect to the frequency deviation, in which K_c and T_c are the PEV charger droop control gain and time constant calculated via $T_c = L_c/R_c$, $\Delta I_{\mathrm{batt}j,t}$ is the battery current deviation. To flexibly maintain different initial SOC levels, the adaptive droop control with a balance SOC Holder proposed in [10] is applied. That is, the adaptive droop gain is given as follows:

1) If $\mathrm{SOC}_{j,t} \leq \mathrm{SOC}_j^{\min}$, then

$$\begin{cases} K_{\mathrm{c}j,t}^{\mathrm{ch}} = K_{j,\max} \\ K_{\mathrm{c}j,t}^{\mathrm{dis}} = 0 \end{cases} \tag{2}$$

2) If $\mathrm{SOC}_{j,t} \geq \mathrm{SOC}_j^{\max}$, then

$$\begin{cases} K_{\mathrm{c}j,t}^{\mathrm{ch}} = 0 \\ K_{\mathrm{c}j,t}^{\mathrm{dis}} = K_{j,\max} \end{cases} \tag{3}$$

3) If $\mathrm{SOC}_j^{\min} < \mathrm{SOC}_{j,t} \leq \mathrm{SOC}_j^{\mathrm{in}}$, then

$$\begin{cases} K_{\mathrm{c}j,t}^{\mathrm{ch}} = \frac{1}{2} K_{j,\max} \left(1 + \sqrt{\frac{\mathrm{SOC}_{j,t} - \mathrm{SOC}_j^{\mathrm{in}}}{\mathrm{SOC}_j^{\min} - \mathrm{SOC}_j^{\mathrm{in}}}} \right) \\ K_{\mathrm{c}j,t}^{\mathrm{dis}} = \frac{1}{2} K_{j,\max} \left(1 - \sqrt{\frac{\mathrm{SOC}_{j,t} - \mathrm{SOC}_j^{\mathrm{in}}}{\mathrm{SOC}_j^{\min} - \mathrm{SOC}_j^{\mathrm{in}}}} \right) \end{cases} \tag{4}$$

4) If $\mathrm{SOC}_j^{\mathrm{in}} < \mathrm{SOC}_{j,t} \leq \mathrm{SOC}_j^{\max}$, then

$$\begin{cases} K_{\mathrm{c}j,t}^{\mathrm{ch}} = \frac{1}{2} K_{j,\max} \left(1 - \sqrt{\frac{\mathrm{SOC}_{j,t} - \mathrm{SOC}_j^{\mathrm{in}}}{\mathrm{SOC}_j^{\max} - \mathrm{SOC}_j^{\mathrm{in}}}} \right) \\ K_{\mathrm{c}j,t}^{\mathrm{dis}} = \frac{1}{2} K_{j,\max} \left(1 + \sqrt{\frac{\mathrm{SOC}_{j,t} - \mathrm{SOC}_j^{\mathrm{in}}}{\mathrm{SOC}_j^{\max} - \mathrm{SOC}_j^{\mathrm{in}}}} \right) \end{cases} \tag{5}$$

where $\mathrm{SOC}_j^{\min}$, $\mathrm{SOC}_j^{\max}$, $\mathrm{SOC}_j^{\mathrm{in}}$, $\mathrm{SOC}_{j,t}$, $K_{\mathrm{c}j,t}^{\mathrm{ch}}$, $K_{\mathrm{c}j,t}^{\mathrm{dis}}$ and $K_{j,\max}$ are minimum SOC, maximum SOC, initial SOC, realtime SOC, charging droop, discharging droop, and maximum droop of j-th PEV's battery. The sign of frequency deviation determines the status of charging or discharging. When the frequency deviation is positive, the PEV will be charged to absorb the extra power from the grid and then $K_{\mathrm{c}j,t} = K_{\mathrm{c}j,t}^{\mathrm{ch}}$. While in the condition of a negative frequency deviation, the power will be injected to the grid and then $K_{\mathrm{c}j,t} = K_{\mathrm{c}j,t}^{\mathrm{dis}}$.

There are many nonlinearities in the dynamic model of a PEV and the balanced SOC control scheme, herein some proper approximations are made to obtain simplified model. Firstly, the SOC is usually limited between 20% and 90% in order to preserve the battery life, so the corresponding open-circuit voltage, $V_{oc}(\mathrm{SOC})$, remains within an approximate constant range for such case [13]. Secondly, the series resistor and transient resistor are usually small, and the battery transient time constant $R_t C_t$ is far larger than the inverter time constant T_c, therefore the voltage drop V_s and V_t can be neglected in comparison with V_{oc}. Based on above approximations, the transfer function model of jth PEV at time t can be written as

$$\frac{\Delta P_{\mathrm{EV}j,t}}{\Delta f} = \frac{K_{\mathrm{EV}j,t}}{1 + sT_{\mathrm{c}j}} \tag{6}$$

where $\Delta P_{\mathrm{EV}j,t}$ is the deviation of the output power of the jth PEV; Δf is the frequency deviation; $K_{\mathrm{EV}j,t} = K_{\mathrm{c}j,t} K_{\mathrm{batt}j}$ is the jth PEV V2G control gain, and $K_{\mathrm{batt}j}$ is the battery gain that is related to the open-circuit voltage, $V_{oc}(\mathrm{SOC})$.

2.2. Aggregated PEVs Model

To accomplish the V2G service, numerous PEVs are required to plug into the power grid. Assume that N PEVs participate in the frequency regulation of each control area, the aggregated model of such PEV fleet is:

$$\Delta P_{\mathrm{EV}} = \sum_{j=1}^{N} \lambda_j \Delta P_{\mathrm{EV}j} \tag{7}$$

where ΔP_{EV} is the deviation of the total output power of all PEVs; λ_j denotes the availability status of jth PEV, with 1 indicating the PEV is available for V2G service and 0 meaning out of V2G service.

By ignoring the impact of differences in time constants of various PEVs on the primary frequency control [23], and considering the communication delays arising in the PEVs' control loop, model (7) can be simplified as

$$\Delta P_{\mathrm{EV}} = \sum_{j=1}^{N} \lambda_j \left\{ e^{-\tau_j s} \frac{K_{\mathrm{EV}j}}{1 + sT_{\mathrm{c}j}} \right\} \Delta f = e^{-\tau s} \frac{K_{\mathrm{EV}}}{1 + sT_{\mathrm{EV}}} \Delta f \tag{8}$$

where K_{EV} is the aggregated time-varying V2G gain and expressed as

$$K_{\mathrm{EV}} = \sum_{j=1}^{N} \lambda_j K_{\mathrm{EV}j} \tag{9}$$

time constants T_{cj} are assumed to be identical $T_{\mathrm{c}j} = T_{\mathrm{EV}}$, since the PFC service provided by the PEVs is insensitive to the variation of time constants [23]; and τ is the time delay in the PEV-based PFC loop, including processing delay for calculation of V2G gain and transmission delay of measured signals. Note that the delays for different PEVs are assumed to be identical for easily constructing the state-space model of LFC.

As mentioned in Section 2.1, the value of the $K_{\mathrm{EV}j}$ is dependent upon the real-time SOC. Furthermore, the values of λ_j are determined by the spatiotemporal diversities of all PEVs. That is, the effective V2G gain is determined by the realtime SOC and the number of charging vehicles. Therefore, according to (9), the aggregated V2G gain, K_{EV}, is time-varying. Actually, it has an upper bound in the case all PEVs are connected to the grid at the same time with maximum droop gain, i.e., $K_{\mathrm{EV}}^{\max} \approx N K_{\mathrm{c}}^{\max} K_{\mathrm{batt}}^{\max}$, where $K_{\mathrm{c}}^{\max}$ and $K_{\mathrm{batt}}^{\max}$ are the maximum droop and equivalent gain, respectively.

Based on the statistical data on spatiotemporal diversities of the PEVs and the relationship between the V2G gain of a PEV and its SOC, one can give the variation curve of the aggregated V2G gain, K_{EV}, which would be rewritten by considering its distribution:

$$K_{\mathrm{EV}}(t) = \bar{K}_{\mathrm{EV}} + \Delta K_{\mathrm{EV}}(t) \tag{10}$$

where $\bar{K}_{\mathrm{EV}}$ is constant and indicates the value that takes up a great portion in whole curve; and ΔK_{EV} is time-varying and denotes the deviation value of $\bar{K}_{\mathrm{EV}}$ from its realtime value, and it will be treated as a part of system disturbance during the development of state-space model. In the following section, the constant value, $\bar{K}_{\mathrm{EV}}$, will be used as the base value for control design due to most value of $K_{\mathrm{EV}}(t)$ closed to its value, and the possible negative influence of deviation value, ΔK_{EV}, on system performance is minimized through the robust design method.

2.3. State-Space Model of the LFC with PEVs and Time Delay

The traditional multi-area LFC scheme in [22] is modified to include the PEVs component for additional primary frequency control. The block diagram of the ith control area in this LFC scheme is shown in Fig. 2. The state-space model is derived for such LFC scheme with distributed PID controller in this part.

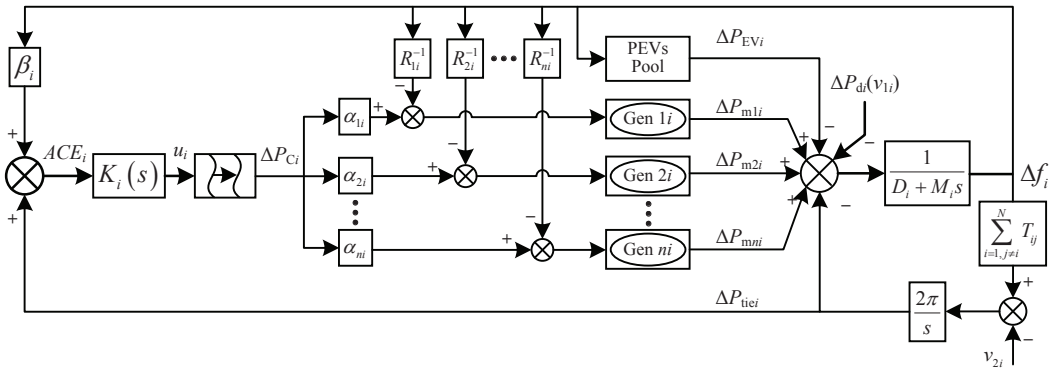

Fig. 2. *Block diagram of control area i in the multi-area LFC scheme with PEVs.*

Based on (8) and (10), the relationship between the ΔP_{EV} and the Δf of area i can be rewritten as the following form:

$$\Delta \dot{P}_{\mathrm{EV}i}(t) = \frac{\bar{K}_{EVi}}{T_{EVi}} \Delta f_i(t-\tau) - \frac{1}{T_{EVi}} \Delta P_{\mathrm{EV}i}(t) + \frac{\Delta K_{EVi}}{T_{EVi}} \Delta f_i(t-\tau) \tag{11}$$

By considering (11) and the dynamic model of original LFC scheme without PEVs reported in [22], the model of the LFC scheme with PEVs and delays concerned in this paper can be expressed as:

$$\begin{cases} \dot{x}_i(t) = A_i x_i(t) + A_{\mathrm{d}i} x_i(t-\tau) \ + B_i u_i(t-h) + F_i \omega_i \\ y_i(t) = C_{\mathrm{y}i} x_i(t) \\ z_i(t) = C_{\mathrm{z}i} x_i(t) \end{cases} \tag{12}$$

where

$$x_i^{\mathsf{T}} = [\Delta f_i, \Delta P_{\mathrm{tie}i}, \Delta P_{\mathrm{EV}i}, \Delta P_{\mathrm{m}1i}, \cdots, \Delta P_{\mathrm{m}ni}, \Delta P_{\mathrm{g}1i}, \cdots, \Delta P_{\mathrm{g}ni}]$$
$$y_i = ACE_i, \ \ z_i^T = [\Delta f, \Delta P_{\mathrm{tie}i}], \ \ u_i = \Delta P_{Ci}$$
$$\omega_i^{\mathsf{T}} = \left[\Delta P_{\mathrm{d}i}, \ \sum_{j=1, j\neq i}^{N} T_{ij} \Delta f_j, \ \Delta K_{EVi} \Delta f_i\right]$$
$$A_i = \begin{bmatrix} A_{11i} & A_{12i} & 0 \\ 0 & A_{22i} & A_{23i} \\ A_{31i} & 0 & A_{33i} \end{bmatrix}, \ A_{\mathrm{d}i} = \begin{bmatrix} A_{\mathrm{d}11i} & 0 & 0 \\ 0 & 0 & 0 \\ 0 & 0 & 0 \end{bmatrix}, \ B_i = \begin{bmatrix} 0 \\ 0 \\ B_{3i} \end{bmatrix}, \ F_i = \begin{bmatrix} F_{11i} \\ 0 \\ 0 \end{bmatrix}$$
$$C_{\mathrm{y}i} = [\beta \ \ 1 \ \ 0 \ \ 0], \ C_{\mathrm{z}i} = [1 \ \ 1 \ \ 0 \ \ 0]$$
$$A_{11i} = \begin{bmatrix} -\frac{D_i}{M_i} & -\frac{1}{M_i} & -\frac{1}{M_i} \\ 2\pi \sum_{j=1, j\neq i}^{N} T_{ij} & 0 & 0 \\ \frac{K_{\mathrm{EV}i}}{T_{\mathrm{EV}i}} & 0 & -\frac{1}{K_{\mathrm{EV}i}} \end{bmatrix}, \ A_{12i} = \begin{bmatrix} \frac{1}{M_i} \cdots \frac{1}{M_i} \\ 0 \ \cdots \ 0 \\ 0 \ \cdots \ 0 \end{bmatrix}, \ A_{31i} = \begin{bmatrix} \frac{-1}{T_{\mathrm{g}1i} R_{1i}} & 0 & 0 \\ \vdots & \vdots & \vdots \\ \frac{-1}{T_{\mathrm{g}ni} R_{ni}} & 0 & 0 \end{bmatrix}$$
$$A_{22i} = -A_{23i} = \mathrm{diag}\left\{-\tfrac{1}{T_{\mathrm{t}1i}}, \cdots, -\tfrac{1}{T_{\mathrm{t}ni}}\right\}, \ \ A_{33i} = \mathrm{diag}\left\{\tfrac{-1}{T_{\mathrm{g}1i}}, \cdots, \tfrac{-1}{T_{\mathrm{g}ni}}\right\}$$
$$A_{\mathrm{d}11i} = \begin{bmatrix} 0 & 0 & 0 \\ 0 & 0 & 0 \\ \frac{K_{\mathrm{EV}i}}{T_{\mathrm{EV}i}} & 0 & 0 \end{bmatrix}, \ B_{3i} = \begin{bmatrix} \frac{\alpha_{1i}}{T_{\mathrm{g}1i}} \\ \cdots \\ \frac{\alpha_{ni}}{T_{\mathrm{g}ni}} \end{bmatrix}, \ F_{11i} = \begin{bmatrix} \frac{-1}{M_i} & 0 & 0 \\ 0 & -2\pi & 0 \\ 0 & 0 & \frac{1}{T_{EVi}} \end{bmatrix}$$

and $\Delta P_{\mathrm{g}ki}$ is the steam valve position deviation, $\Delta P_{\mathrm{m}ki}$ is the mechanical power change, $\Delta P_{\mathrm{tie}i}$is the tie-line exchange power, $\Delta P_{\mathrm{d}i}$ is the load power change, $T_{\mathrm{g}ki}$ is the governor time constant, $T_{\mathrm{t}ki}$ is the turbine time constant, R_{ki} is the speed droop characteristic, M_i is angular momentum, D_i is

the load damping coefficient, β_i is the frequency bias factor, α_{ki} is the participation factor, T_{ij} is the synchronizing torque coefficient between area i and j, and τ and h are the time delay of PEVs loop and LFC loop, respectively, in area i. Note that it is assumed that the time delay in the original LFC loop and the PEVs loop are identical, $\tau = h$, for simplifying the analysis in the following sections.

The following PID-type LFC scheme is designed:

$$u_i(t) = -K_{Pi}ACE_i - K_{Ii}\int ACE_i \mathrm{d}t - K_{Di}\frac{\mathrm{d}}{\mathrm{d}t}ACE_i \tag{13}$$

where K_{Pi}, K_{Ii}, and K_{Di} are the PID gains to be determined; and ACE_i is the area control error of area i and is obtained as

$$ACE_i = \beta_i \Delta f_i + \Delta P_{\mathrm{tie}i} \tag{14}$$

By integrating (13) to (11) and following the similar line in [22], the closed-loop state-space equations are as follows

$$\begin{cases} \dot{\bar{x}}_i(t) = \bar{A}_i\bar{x}_i(t) + \bar{A}_{\mathrm{d}i}\bar{x}_i(t-\tau_i(t)) + \bar{B}_{\mathrm{w}i}\omega_i \\ \bar{y}_i(t) = \bar{C}_{\mathrm{y}i}\bar{x}_i(t) + \bar{D}_i\omega_i \\ \bar{z}_i(t) = \bar{C}_{\mathrm{z}i}\bar{x}_i(t) \end{cases} \tag{15}$$

where

$$\bar{A}_i = \begin{bmatrix} A_i & 0 \\ C_{\mathrm{y}i} & 0 \end{bmatrix},\ \bar{A}_{\mathrm{d}i} = -\bar{B}_iK_i\bar{C}_{\mathrm{y}i} + \begin{bmatrix} A_{\mathrm{d}i} & 0 \\ 0 & 0 \end{bmatrix},\ \bar{B}_{\mathrm{w}i} = \bar{F}_i - \bar{B}_iK_i\bar{D}_i,\ K_i = [K_{\mathrm{P}i}\ \ K_{\mathrm{I}i}\ \ K_{\mathrm{D}i}]$$

$$\bar{C}_{\mathrm{z}i} = \begin{bmatrix} \zeta_{1i}C_{\mathrm{z}i} & 0 \\ 0 & \zeta_{2i} \end{bmatrix},\ \bar{B}_i = \begin{bmatrix} B_i \\ 0 \end{bmatrix},\ \bar{F}_i = \begin{bmatrix} F_i \\ 0 \end{bmatrix},\ \bar{C}_{\mathrm{y}i} = \begin{bmatrix} C_{\mathrm{y}i} & 0 \\ 0 & 1 \\ C_{\mathrm{y}i}A_i & 0 \end{bmatrix},\ \bar{D}_i = \begin{bmatrix} 0 \\ 0 \\ C_{\mathrm{y}i}F_i \end{bmatrix}$$

and $\bar{z}_i = [\zeta_{1i}z_i^{\mathsf{T}} \quad \zeta_{2i}\int y_i^{\mathsf{T}}]^{\mathsf{T}}$, ζ_{1i} and ζ_{2i} are weights which can be chosen to get a desired performance.

If the communication delay in PEVs loop is not included, then the new closed-loop state-space equation can be easily obtained from (15) by setting $\bar{A}_i = \begin{bmatrix} A_i + A_{di} & 0 \\ C_{\mathrm{y}i} & 0 \end{bmatrix}$ and $\bar{A}_{\mathrm{d}i} = -\bar{B}_iK_i\bar{C}_{\mathrm{y}i}$.

3. Robust Controller Design

In this section, the delay-dependent H_∞ performance analysis is conducted to derive a criterion. Then, based on the criterion, tuning the controller gains is transformed into an optimization problem solved by PSO algorithm.

3.1. Delay-dependent H_∞ Performance Analysis

The closed-loop systems for different control areas shown in (15) can be described by the following general form:

$$\begin{cases} \dot{x}(t) = Ax(t) + A_dx(t-h) + (B_w - BKD)\omega(t) \\ z(t) = C_{\mathrm{z}}x(t) \end{cases} \tag{16}$$

By using the Lyapunov-Krasovskii functional method, the relationships among the delay bound, the robust performance index, and the control gains can be described by the following criterion.

Theorem 1: Consider the closed-loop system (16), for the delay bound h, the H_∞ performance index γ, and the controller gains $K = [K_\mathrm{P}\ K_\mathrm{I}\ K_\mathrm{D}]$, if there exist symmetric matrices P, Q, and R, such that the following LMIs holds

$$P > 0,\ Q > 0,\ R > 0 \tag{17}$$

$$\begin{aligned}\Phi = Sym\left\{\begin{bmatrix} e_1 \\ he_3 \end{bmatrix}^T P \begin{bmatrix} e_s \\ e_1 - e_2 \end{bmatrix}\right\} - \begin{bmatrix} e_1 - e_2 \\ e_1 + e_2 - 2e_3 \end{bmatrix}^T \begin{bmatrix} R & 0 \\ 0 & 3R \end{bmatrix} \begin{bmatrix} e_1 - e_2 \\ e_1 + e_2 - 2e_3 \end{bmatrix} \\ + e_1^T Q e_1 - e_2^T Q e_2 + h^2 e_s^T R e_s + e_1^T C_z^T C_z e_1 - \gamma^2 e_4^T e_4 \\ < 0\end{aligned} \tag{18}$$

where $e_s = \big[A, A_d{-}BKC_\mathrm{y}, 0, B_w{-}BKD\big], e_1 = \big[I, 0, 0, 0\big], e_2 = \big[0, I, 0, 0\big], e_3 = \big[0, 0, I, 0\big], e_4 = \big[0, 0, 0, I\big]$, then the system is stable and has H_∞ performance index, γ, against a non-zero disturbance for any delays smaller than h.

Proof: Choose an LKF candidate as follows:

$$V(x_t) = \begin{bmatrix} x(t) \\ \int_{t-h}^{t} x(s)ds \end{bmatrix}^T P \begin{bmatrix} x(t) \\ \int_{t-h}^{t} x(s)ds \end{bmatrix} + \int_{t-h}^{t} x^T(s) Q x(s) ds + h \int_{-h}^{0} \int_{t+\theta}^{t} \dot{x}^T(s) R \dot{x}(s) ds d\theta$$

where P, Q, and R are symmetrical matrices. It can be found that the positive of the LKF, ($V(x_t) > 0, \forall x_t \neq 0$), can be ensured if LMI (17) holds.

Calculating the derivative of LKF and using Wirtinger-based integral inequality [24] yields

$$\begin{aligned}&\dot{V}(x_t) \\ &= 2\begin{bmatrix} x(t) \\ \int_{t-h}^{t} x(s)ds \end{bmatrix}^T P \begin{bmatrix} \dot{x}(t) \\ x(t) - x(t-h) \end{bmatrix} + x^T(t) Q x(t) - x^T(t-h) Q x(t-h) + h^2 \dot{x}^T(t) R \dot{x}(t) \\ &\quad - h \int_{t-h}^{t} \dot{x}^T(s) R \dot{x}(s) ds \\ &\leq 2\begin{bmatrix} x(t) \\ \int_{t-h}^{t} x(s)ds \end{bmatrix}^T P \begin{bmatrix} \dot{x}(t) \\ x(t) - x(t-h) \end{bmatrix} + x^T(t) Q x(t) - x^T(t-h) Q x(t-h) + h^2 \dot{x}^T(t) R \dot{x}(t) \\ &\quad - \begin{bmatrix} x(t) - x(t-h) \\ x(t) + x(t-h) - 2\int_{t-h}^{t} \frac{x(s)}{h} ds \end{bmatrix}^T \begin{bmatrix} R & 0 \\ 0 & 3R \end{bmatrix} \begin{bmatrix} x(t) - x(t-h) \\ x(t) + x(t-h) - 2\int_{t-h}^{t} \frac{x(s)}{h} ds \end{bmatrix}\end{aligned}$$

By defining the following notations

$$\begin{aligned} \zeta(t) &= \left[x(t),\ x(t-h),\ \int_{t-h}^{t} \frac{x(s)}{h} ds, \omega(t)\right] \\ \dot{x}(t) &= e_s \zeta(t),\ \ e_s = \big[A, A_d, 0, B_{w1} - BKD\big] \\ x(t) &= e_1 \zeta(t),\ \ e_1 = \big[I, 0, 0, 0\big] \\ x(t-h) &= e_2 \zeta(t),\ \ e_2 = \big[0, I, 0, 0\big] \\ \int_{t-h}^{t} \frac{x(s)}{h} ds &= e_3 \zeta(t),\ \ e_3 = \big[0, 0, I, 0\big] \\ \omega(t) &= e_4 \zeta(t),\ \ e_4 = \big[0, 0, 0, I\big] \end{aligned}$$

It follows (18) that

$$\dot{V}(x_t) + z^T(t)z(t) - \gamma^2\omega^T(t)\omega(t) \leq \zeta^T(t)\Phi\zeta(t) \leq 0 \tag{19}$$

where Φ is defined in (18). Thus, based on (19) and $V(x_0) = 0$, $V(x_\infty) \geq 0$, the following holds

$$\int_0^\infty \left[z^T(s)z(s) - \gamma^2\omega^T(s)\omega(s)\right]ds \leq V(x_0) - V(x_\infty) \leq 0$$

Therefore,

$$\sqrt{\frac{\int_0^\infty z^T(s)z(s)ds}{\int_0^\infty \omega^T(s)\omega(s)ds}} \leq \gamma$$

which means the the system is stable and has a H_∞ performance index, γ. This completes the proof.

Remark 1: Theorem 1 gives the relationships among h, γ, and K. Based on Theorem 1, for the fixed delay bound h and the controller gains K, one can find the minimal value of the performance index $\gamma_{\min}$. That is, $\gamma_{\min}$ is a function of h and K:

$$\gamma_{\min} = f(h, K) = f(h, K_{\mathrm{P}}, K_{\mathrm{I}}, K_{\mathrm{D}}) \tag{20}$$

How to calculate $\gamma_{\min}$ for fixed h and K can be found in [22] and is omitted here.

3.2. PSO-Based Controller Gain Tuning

For a built communication channel, the time delay upper bound can be estimated from the transmitted data with time stamp. Then, for such delay bound, different controller gains lead to different performance indices calculated via (20). Therefore, to provide the optimal robust performance for a preset time delay, tuning the control gains can be realised by solving the following optimization problem:

$$\begin{aligned} \text{Minimize}: \quad & \gamma_{\min} = f(h, K_{\mathrm{P}}, K_{\mathrm{I}}, K_{\mathrm{D}}) \\ \text{subject to}: \quad & K_{Pmin} \leq K_P \leq K_{Pmax} \\ & K_{Imin} \leq K_I \leq K_{Imax} \\ & K_{Dmin} \leq K_D \leq K_{Dmax} \end{aligned} \tag{21}$$

The problem can be solved by different optimization algorithms. This paper chooses the PSO algorithm as it has been widely used due to its decent performance in numerical optimization [25, 26]. The flowchart of the PID gains tuning is shown in Fig. 3.

In the initialization step, the following parameters should be given or calculated:

- Set the time delay upper bound, h.
- Set position bounds, $X_{\min}$ and $X_{\max}$, velocity bounds, $V_{\min}$ and $V_{\max}$, and population size, N; and obtain random positions X_0 within $[X_{\min}, X_{\max}]$ (i.e., N sets of gains $K = [K_P\ K_I\ K_D]$) and the velocities V_0 within $[V_{\min}, V_{\max}]$.
- Set the maximal iteration times, $k_{\max}$, and the initial iteration times $i = 0$.
- Evaluate the fitness (i.e., H_∞ performance index, $\gamma_{\min}$ shown in (20)) for N particles, $f(h, X_{0,j})$, $j = 1, 2, \cdots, N$, via Theorem 1 and Remark 1.

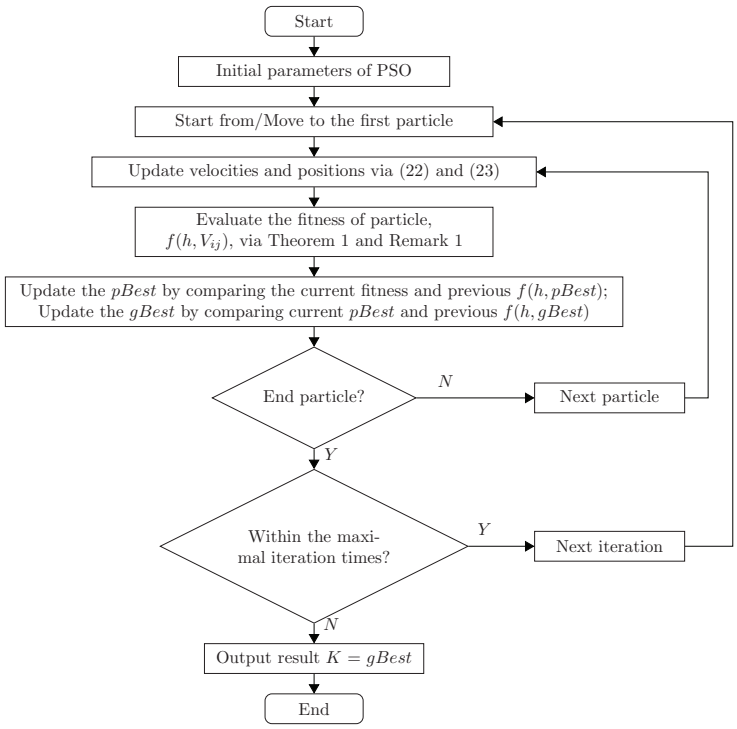

Fig. 3. *Simplified flowchart of the PID tuning.*

- Find the best position for each particle, $pBest$, and the best position within all particles, $gBest$, i.e., set $f(h, pBest_j) = f(h, X_{0,j}), j = 1, 2, \cdots, N$ and $pBest = X_0$, and set $gBest = X_{o,k}, k \in \{1, 2, \cdots, N\}$ such that $f(h, gBest) = \min f(h, X_{0,j}), j = 1, 2, \cdots, N$.

In the step of updating the velocities and the positions, the following conditions are applied:

$$V_{i+1} = \begin{cases} V_{\min}, & \text{if } V_{i+1} < V_{\min} \\ wV_i + c_1 \cdot \text{rand} \cdot (pBest - X_i) + c_2 \cdot \text{rand} \cdot (gBest - X_i), & \text{if } V_{i+1} \in [V_{\min}, V_{\max}] \\ V_{\max}, & \text{if } V_{i+1} > V_{\max} \end{cases} \quad (22)$$

where V_i and V_{i+1} are the velocities in ith and $(i+1)$th iteration, w is the inertia weight, c_1 and c_2 are the acceleration constants, and rand is a value randomly generated between 0 and 1; and

$$X_{i+1} = \begin{cases} X_{\min}, & \text{if } X_{i+1} < X_{\min} \\ X_i + V_{i+1}, & \text{if } X_{i+1} \in [X_{\min}, X_{\max}] \\ X_{\max}, & \text{if } X_{i+1} > X_{\max} \end{cases} \quad (23)$$

where X_i and X_{i+1} are the positions in ith and $(i+1)$th iteration.

Remark 1. Although our previous research [22] has proposed the delay-dependent LFC scheme design method for multi-area power systems, the work of this paper is different from two aspects. For one thing, the power systems concerned in [22] do not include the PEVs. For another, the PSO algorithm is used to tune the control gains and it is simpler than the one applied in [22].

4. Case Studies

Case studies are carried out based on a three-area interconnected LFC scheme, which is constructed by introducing the PEVs into the traditional three-area LFC discussed in [27]. The structure and the parameters of each area for the original LFC scheme part are given in [27]. In each control area, assume that 12,500 PEVs are participating in the V2G service, and the parameters of each PEV are tabulated in Table 1 [10]. It is assumed that the PEVs' users start to work at 09:00 and get off work at 17:00. The initial SOC and the desired SOC are uniformly distributed between 30% and 50% and between 80% and 90%, respectively. The charging start time and charging end time follow the normal distribution $N(\mu, \sigma^2)$ with $\mu = 9$, $\sigma = 0.5$, and $\mu = 17$, $\sigma = 0.5$, respectively [28]. The simulation tests are carried out under the cases of step load changes and the long-term random demands. In this section, two PID controllers are designed via the proposed simplified model and robust design method, and then simulation studies are performed based on the more detailed nonlinear model. All calculations and simulations in the followings are carried out by using Matlab R2014a running on a PC with 2.80-GHz Intel Core i5 CPU, 8GB RAM, and Windows 7 64-bit Ultimate.

Table 1 Parameters of PEVs

Parameters	Value
Base power [MW]	1000
Battery capacity (E_r) [Ah]	66.2
Battery transient resistor (R_s) [Ω]	0.074
Battery transient resistor (R_t) [Ω]	0.047
Battery transient capacitor (C_t) [F]	703.6
Charging/discharging efficiency	0.92/0.92
PEV charger time constant (T_c) [s]	0.05
Maximum V2G power [kW]	5
Maximum V2G gain ($K_{\max}$) [pu/Hz]	4.8×10^{-5}
SOC limits ($\mathrm{SOC}_{\max}/\mathrm{SOC}_{\min}$)	0.90/0.10

4.1. Robust PID controllers design

Based on the simplified state-space model developed in Section 2, two PID controllers are designed respectively for the concerned LFC scheme with and without considering the communication delay in the PEVs primary frequency control loops.

The gain of the simplified and aggregated PEVs model, K_{EV}, is estimated at first. Based on the PEVs related parameters aforementioned and the probability distributions of the plug-in/out time (shown in Fig. 4(a)), one can estimate the changing curve of the number of the EVs plugged-in the grid and of the PEVs model's gain in the large range, as shown in the Fig. 4(b) and (c). It can be found that most value of K_{EV} is around 0.3, thus the nominal value of K_{EV} (i.e., $\bar{K}_{\mathrm{EV}}$ in state-space model) is chose to be 0.3 for controller design and the deviation value, $K_{\mathrm{EV}} - \bar{K}_{\mathrm{EV}}$, is considered as the disturbance part.

The initial PSO parameters mentioned in Section 3.2 are given as $X_{\max} = 1$, $X_{\min} = -1$; $V_{\max} = 1$, $V_{\min} = -1$; $N = 50$; $k_{\max} = 50$; $w = 0.4$, $c_1 = c_2 = 2$. The upper delay bounds in the LFC loops for each area are set to 4s and those in the PEVs loops are set to 0 (Case I) or 4s (Case II). The controller gains for two cases, together with the one reported in [22], are listed in Table 2, in which C1 is for the case of LFC without PEVs, C2 is for the case that the LFC scheme includes

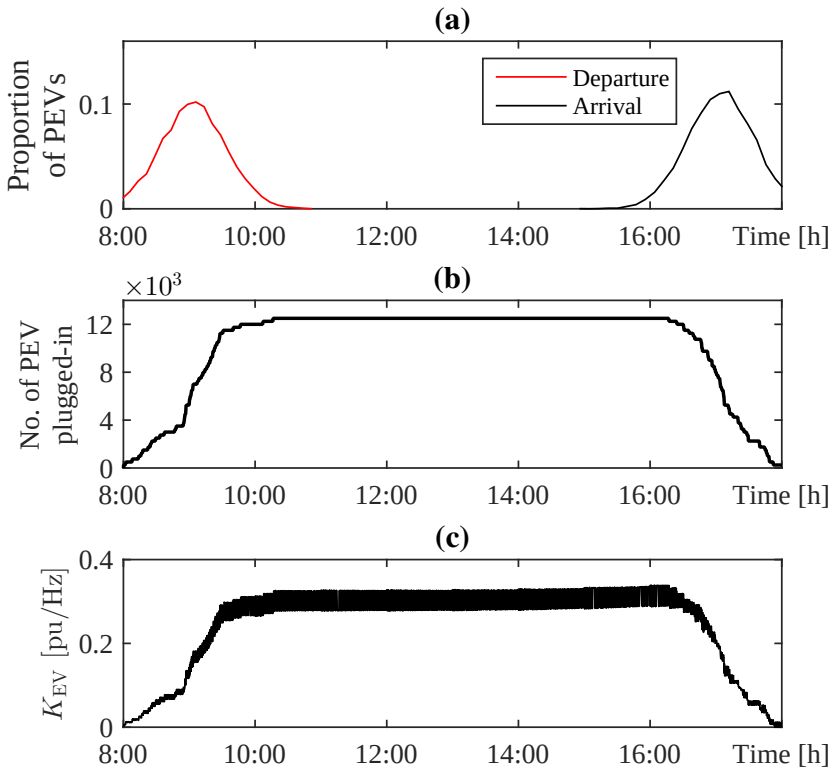

Fig. 4. *Information for estimating K_{EV}. (a) the distributions of plug-in/out time; (b) the number of the PEVs connected to grid; and (c) the aggregated V2G gain*

the PEVs without considering the PEVs loop delays, and C3 is designed considering both PEVs and the time delays in control loops.

Table 2 The PID Controller Parameters

Controllers	Areas	K_P	K_I	K_D
C1 [22]	1	-0.0669	0.0615	0.0311
	2	-0.0305	0.0885	0.0325
	3	-0.0704	0.0688	0.0302
C2	1	0.1305	0.1700	0.0349
	2	0.2163	0.2065	0.0597
	3	0.1759	0.1868	0.0435
C3	1	-0.1499	0.1519	-0.0328
	2	-0.0825	0.1399	-0.0087
	3	-0.1516	0.1116	-0.0293

4.2. Simulation verification: Step load disturbance

Apply the MATLAB/Simulink platform to construct the detailed closed-loop system by considering necessary nonlinear dynamics, such as the generation rate constraints (0.05 pu/min and 0.20 pu/min [22]), and the nonlinear model of electric vehicles described in Section 2. The designed controllers are firstly tested in the presence of step changes of load demands occurring at $0.2\mathrm{s}$, namely, $\Delta P_{\mathrm{d1}} = 0.10\mathrm{pu}$, $\Delta P_{\mathrm{d2}} = 0.08\mathrm{pu}$, $\Delta P_{\mathrm{d3}} = 0.05\mathrm{pu}$.

For scenario 1, the cases for the LFC without PEVs and including PEVs but without PEVs loop delays are compared to verify the contribution of PEVs to frequency regulation. Controllers C1 and C2 are used for those cases respectively. The responses of frequency deviation, ACE, and power exchanges for area 1 are shown in Fig. 5. The results demonstrate that the PEVs can improve the transient performance, shortening the undershoot and settling time. The responses for areas 2 and 3 lead to similar results and are omitted here.

For scenario 2, the time delay possibly exists in the PEVs control loops, as mentioned in Section 1, thus it's necessary to test the controllers that are designed considering and without considering delays (C2 and C3, respectively). Assume that 4s of delays are applied into the main LFC loop and the PEV control loop during the simulation. Fig. 6 shows the C2 cannot stabilize the closed-loop system while the C3 can make it in the presence of time delays and guarantee the dynamic performance. It demonstrates the necessity of considering the delays during the controller design stage.

For scenario 3, different gain values K_{EV} are selected to assess the robustness of the designed PID controllers against the uncertainties and time delay in PEVs charging. To easily evaluate dynamic performances of the controllers, three commonly used performance indices are adopted, i.e., integral squared error (ISE), integral of the time multiplied absolute value of the error (ITAE), and integral absolute error (IAE):

$$\begin{aligned}
\mathrm{ISE} &= \int_0^{100} \left(\Delta f_1^2 + \Delta f_2^2 + \Delta f_3^2\right) \mathrm{d}t \\
\mathrm{ITAE} &= \int_0^{100} t\left(|\Delta f_1| + |\Delta f_2| + |\Delta f_3|\right) \mathrm{d}t \\
\mathrm{IAE} &= \int_0^{100} \left(|\Delta f_1| + |\Delta f_2| + |\Delta f_3|\right) \mathrm{d}t
\end{aligned}$$

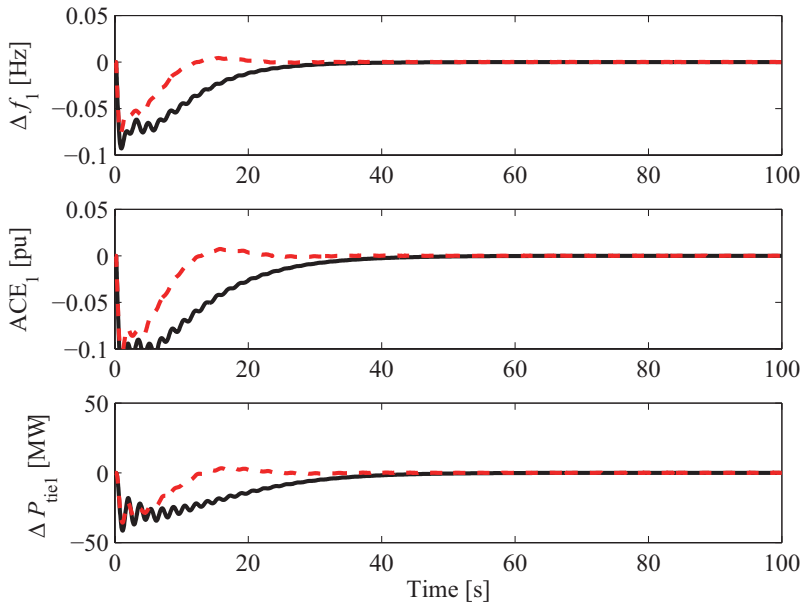

Fig. 5. *The responses of area 1 for scenario 1 (black line: C1, red dashed line: C2).*

The performance indices of frequency deviation for different K_{EV} are listed in Table 3 and the corresponding time-domain simulations are illustrated in Fig. 7. It is shown that the proposed controller can still provide acceptable dynamic performance when the K_{EV} is different from the based value (0.3). That is to say, the proposed controller has desired robustness against to the parameter uncertainties arising from driving behavior of the PEVs.

Table 3 Performance indices for the cases with and without PEVs

Indices	K_{EV}								Without
	0.05	0.10	0.15	0.20	0.25	0.30	0.35	0.40	PEVs
ISE	0.121	0.113	0.106	0.101	0.096	0.092	0.088	0.086	0.156
ITAE	20.411	16.944	14.211	12.350	10.997	9.440	9.198	10.849	27.920
IAE	2.334	2.146	1.986	1.858	1.752	1.651	1.615	1.660	2.985

4.3. Simulation verification: Long-term random load changes

Simulation studies with respect to long-term random load disturbances are conducted to verify the effectiveness of the proposed controller. In order to reduce the simulation time, for the simulation study under the case of long-term random demand change, those PEVs are divided into 200 groups, and the ones in each group have identical initial SOC, charging start time, and charging end time with the distributions given in the beginning of this section. Assume that each area has long-term (several hours) random load disturbances within $[-0.1\mathrm{pu},\ 0.1\mathrm{pu}]$. The time delays in LFC control loop and PEV control loop are random with respect to time, and uniformly generated within $[2\mathrm{s},\ 6\mathrm{s}]$ and $[1\mathrm{s},\ 3\mathrm{s}]$, respectively. Other simulation conditions are the same as in Section 4.2.

For scenario 4, two cases (only LFC and LFC with PEVs) are tested under the above operation condition. The frequency deviation and tie-line power exchange of area 1 are shown in Fig. 8. The figure shows that the bounds of frequency deviation and power exchanges for the case with PEVs

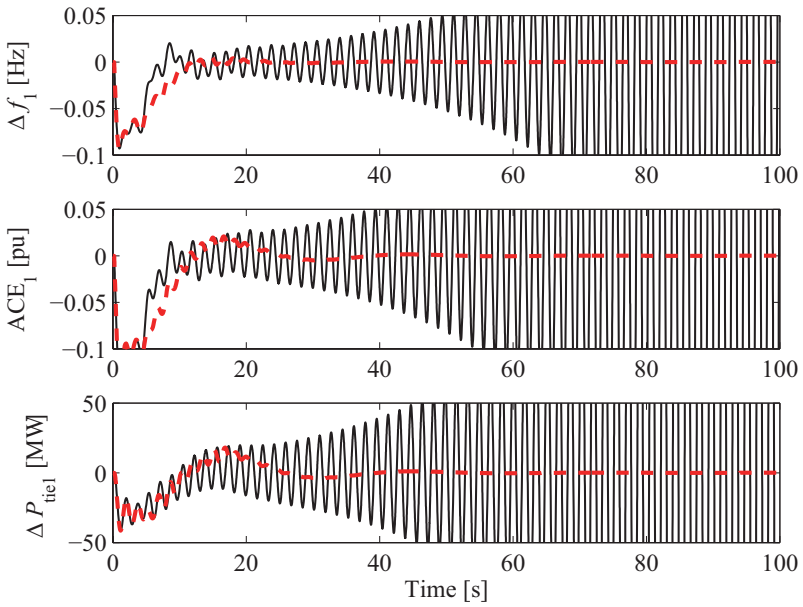

Fig. 6. *The responses of area 1 for scenario 2 (black line: C2; red dashed line: C3).*

are smaller than those for the case without PEVs. To clearly compare the results, the absolute values of frequency deviation (AVFD) and tie-line power exchanges (AVPE) of area 1 are given in Table 4. It is observed that smaller AVFD/AVPE for the case with PEVs has a bigger percentage than that for the case without PEVs. For example, about 93% of the AVFD is less than 0.02Hz and more than 93% of the AVPE is within the range of $0\sim10$MW for the case with PEVs, whereas only 86% of the AVFD falls in the interval of $0\sim0.02$Hz and 66% of the AVPE is within in the range of $0\sim10$MW for the case without PEVs. Meanwhile, Fig. 8 gives the SOC variations of randomly selected three PEV groups (from initial SOC within $[30\%,\ 50\%]$ to the desired SOC within $[80\%,\ 90\%]$), which shows that the charging demands of the PEV customers are satisfied within the plugged-in duration.

Table 4 Probability of the AVFD within an interval of 0.01Hz and the AVPE within an interval of 5MW

Percentage (%)		With PEVs	Without PEVs
AVFD (Hz)	$0\sim0.01$	64.55	59.39
	$0.01\sim0.02$	29.05	27.34
	$0.02\sim0.03$	5.69	10.36
	$0.03\sim0.04$	0.64	2.49
	$0.04\sim0.05$	0.03	0.39
AVPD (MW)	$0\sim5$	68.63	39.37
	$5\sim10$	24.51	26.76
	$10\sim15$	5.55	16.28
	$15\sim20$	1.16	1.10
	$20\sim25$	0.12	4.63

The simulation tests for other cases, such as the uncertainties of parameters (including but not limited to K_{EV}), are carried out to verify the robustness, as discussed in [22]. The detailed results are omitted here due to the page limitation.

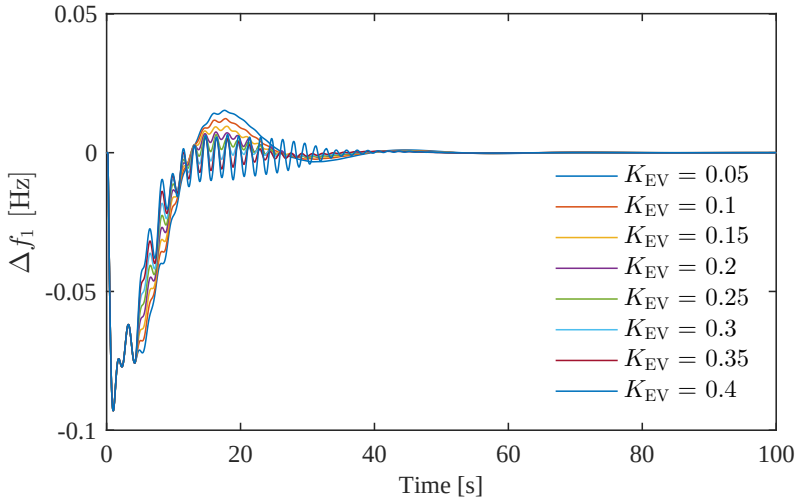

Fig. 7. *Time-domain responses of frequency deviation in area 1 with different values of* K_{EV}.

5. Conclusion

This paper has developed a robust PID-type LFC scheme for multi-area power systems with the V2G service provided by the PEVs, considering the uncertainties caused by the drivers' behaviors and the impact of communication delays appearing in the measurement and the control loops.

A Thevenin equivalent circuit based model with adaptive droop control for each PEV has been developed considering the SOC information of PEV's battery. Then, an aggregated model of large-scale PEVs, namely, a simplified first-order model with a time-varying V2G gain, has been developed considering communication delays and uncertainties of drivers' behaviors. After dividing the time-varying V2G gain into two parts and combining the time-varying part with load demand changes, the closed-loop LFC scheme has been modeled as delay-dependent state-space equations.

Based on the proposed model, a robust PID design condition has been constructed through the H_∞ control theory to guarantee the stability of system with time-varying delays within the preset bounds and to provide desired robustness against the uncertainties of aggregated model of PEVs and load disturbances. Then, the controller parameters have been calculated from such condition by using the LMI solver and the PSO algorithm. The simulation studies based on a three-area LFC system have demonstrated the developed LFC scheme provides good robust dynamic performance against the uncertainties, the disturbances, and the time-varying communication delays. Moreover, for either the short step load change or the long-term random road demand, the V2G service provided by the PEVs has contributions to the frequency regulation and has improved the dynamic performance of the closed-loop LFC system.

In the future work, the development of LFC scheme for smart gird containing renewable energies, energy storage systems, and more controllable loads, including but not limited to the PEVs, will be investigated. Moreover, more comprehensive real driving patterns from practical operations will be considered during the development of LFC schemes.

6. References

[1] Kundur, P.: *Power System Stability and Control*, New York: McGrawHill, 1994.

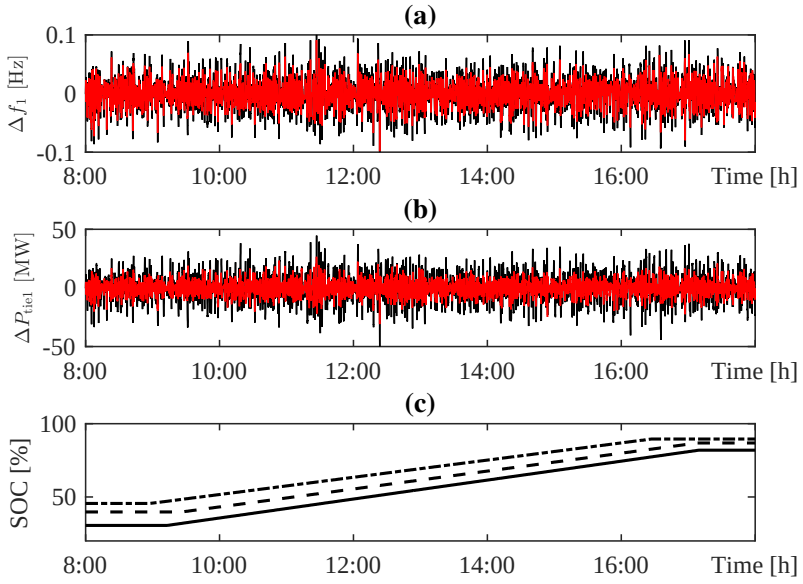

Fig. 8. *(a)Frequency deviation in area 1; (b)Tie-line power in area 1 (black line: without PEVs, red line: with PEVs); (c)The SOC variations of randomly selected three PEV groups.*

[2] Luo, Z., Hu, Z., Song, Y., Xu, Z., Lu, H.: 'Optimal coordination of plug-in electric vehicles in power grids with cost-benefit analysis Part I: Enabling techniques', *IEEE Trans. Power Syst.*, 2013, 28, **(4)**, pp. 3546–3555

[3] Kumar, K. N., Sivaneasan, B., Cheah, P., So, P., Wang, D.: 'V2G capacity estimation using dynamic EV scheduling', *IEEE Trans. Smart Grid*, 2014, 5, **(2)**, pp. 1051–1060

[4] Ma, Y., Houghton, T., Cruden, A., and Infield, D.: 'Modeling the benefits of Vehicle-to-Grid technology to a power system', *IEEE Trans. Power Syst.*, 2012, 27, **(2)**, pp. 1012–1020

[5] Seyedmahdi, I., Garcia-Gonzalez, P., Frłas, P.: 'An aggregate model of plug-in electric vehicles for primary frequency control', *IEEE Trans. Power Syst.*, 2015, 30, **(3)**, pp. 1475-1482

[6] Seyedmahdi, I., Garcia-Gonzalez, P., Frłas, P., Ramirez-Elizondo, L.: 'An aggregate model of plug-in electric vehicles including distribution network characteristics for primary frequency control', *IEEE Trans. Power Syst.*, 2016, in press

[7] Ota, Y., Taniguchi, H., Nakajima, T., Liyanage, K. M., Baba, J., Yokoyama, A.: 'Autonomous distributed V2G (vehicle-to-grid) satisfying scheduled charging', *IEEE Trans. Smart Grid*, 2012, 3, **(1)**, pp. 559–564

[8] Meng, J., Mu, Y., Jia, H., Wu, J., Yu, X., Qu, B.: 'Dynamic frequency response from electric vehicles considering travelling behavior in the Great Britain power system', *Applied Energy*, 2016, 162, pp. 966-979

[9] Yang, H., Chung, C., Zhao, J.: 'Application of plug-in electric vehicles to frequency regulation based on distributed signal acquisition via limited communication', *IEEE Trans. Power Syst.*, 2013, 28, **(2)**, pp. 1017–1026

[10] Liu, H., Hu, Z., Song, Y., and Lin, J: 'Decentralized vehicle-to-grid control for primary frequency regulation considering charging demands', *IEEE Trans. Power Syst.*, 2013, 28, **(3)**, pp. 3480–3489

[11] Brooks, A. N.: *Vehicle-to-grid demonstration project: Grid regulation ancillary service with a battery electric vehicle*. California Environmental Protection Agency, Air Resources Board, Research Division, 2002

[12] Vachirasricirikul, S., Ngamroo, I.: 'Robust controller design of heat pump and plug-in hybrid electric vehicle for frequency control in a smart microgrid based on specified-structure mixed H_2H_∞ control technique', *Applied Energy*, 2011, 88, pp. 3860-3868

[13] Pillai, J. R., Bak-Jensen, B.: 'Integration of vehicle-to-grid in the western Danish power system', *IEEE Trans. Sustain. Energy*, 2011, 2, **(1)**, pp. 12–19

[14] Zhong, J., He, L., Li, C., Cao, Y., Wang, J., Fang, B., Zeng, L., Xiao, G.: 'Coordinated control for large-scale EV charging facilities and energy storage devices participating in frequency regulation', *Applied Energy*, 2014, 123, pp. 253-262

[15] Vachirasricirikul, S., Ngamroo, I.: 'Robust LFC in a smart grid with wind power penetration by coordinated V2G control and frequency controller', *IEEE Trans. Smart Grid*, 2014, 5, **(1)**, pp. 371-380

[16] Liu, H., Hu, Z., Song, Y., Wang, J., Xie, X.: 'Vehicle-to-Grid Control for Supplementary Frequency Regulation Considering Charging Demands', *IEEE Trans. Power Syst.*, 2015, 30, **(6)**, pp. 3110-3119

[17] Pham T. N., Trinh H., Hien L. V.: 'Load frequency control of power systems with electric vechicle and diverse transmission links using distributed functional observers', *IEEE Trans. Smart Grid*, 2015, in press

[18] Yao, W., Zhao, J., Wen, F., Xue, Y., Ledwich, G.: 'A hierarchical decomposition approach for coordinated dispatch of plug-in electric vehicles', *IEEE Trans. Power Syst.*, 2013, 28, **(3)**, pp. 2768–2778

[19] Yu, X. Tomsovic, K.: 'Application of linear matrix inequalities for load frequency control with communication delays', *IEEE Trans. Power Syst.*, 2004, 19, **(3)**, pp. 1508–1515

[20] Jiang, L., Yao, W., Wu, Q., Wen, J., and Cheng, S.: 'Delay-dependent stability for load frequency control with constant and time-varying delays', *IEEE Trans. Power Syst.*, 2012, 27, **(2)**, pp. 932–941

[21] Zhang, C., Jiang, L., Wu, Q., He, Y., Wu, M.: 'Further results on delay-dependent stability of multi-area load frequency control', *IEEE Trans. Power Syst.*, 2013, 28, **(4)**, pp. 4465–4474

[22] Zhang, C., Jiang, L., Wu, Q., He, Y., Wu, M.: 'Delay-dependent robust load frequency control for time delay power systems', *IEEE Trans. Power Syst.*, 2013, 28, **(3)**, pp. 2192–2201

[23] Mu, Y., Wu, J., Ekanayake, J., Jenkins, N., Jia, H.: 'Primary frequency response from electric vehicles in the Great Britain power system', *IEEE Trans. Smart Grid*, 2013, 4, **(2)**, pp. 1142-1150

[24] Seuret, A., Gouaisbaut, F.: 'Wirtinger-based integral inequality: application to time-delay systems', *Automatica*, 2013, 49, **(9)**, pp. 2860–2866

[25] Ting, T., Rao, M., Loo, C.: 'A novel approach for unit commitment problem via an effective hybrid particle swarm optimization', *IEEE Trans. Power Syst.*, 2006, 21, **(1)**, pp. 411–418

[26] Zhao, J., Wen, F., Dong, Z. Y., Xue, Y.,Xue, K. P.: 'Optimal dispatch of electric vehicles and wind power using enhanced particle swarm optimization', *IEEE Trans. Ind. Inf.*, 2012, 8, **(4)**, pp. 889–899

[27] Rerkpreedapong, D., Hasanovic, A., Feliachi, A.: 'Robust load frequency control using genetic algorithms and linear matrix inequalities', *IEEE Trans. Power Syst.*, 2003, 18, **(2)**, pp. 855–861

[28] Luo, Z., Song, Y., Hu, Z., Xu, Z., Yang, X., Zhan, K.: 'Forecasting charging load of plug-in electric vehicles in China," in *Proc. IEEE Power and Energy Society General Meeting*, 2011, pp. 1-8.

[29] Luo, X., Xia, S., Chan, K. W.: 'A decentralized charging control strategy for plug-in electric vehicles to mitigate wind farm intermittency and enhance frequency regulation', *J. Power Sources*, 2014, 248, 604–614